Journal of Medical Virology

WILEY

JOURNAL OF MEDICAL VIROLOGY

RESEARCH ARTICLE OPEN ACCESS

SARS-CoV-2 Productively Infects Human Hepatocytes and Induces Cell Death

Chunkyu Ko[1,2] | Cho-Chin Cheng[1] | Daniele Mistretta[1] | Shubhankar Ambike[1] | Julia Sacherl[1] | Stoyan Velkov[1] | Bo-Hung Liao[1] | Romina Bester[1] | Merve Gültan[1] | Olga Polezhaeva[1] | Alexander Herrmann[1] | Constanze A. Jakwerth[3] | Carsten B. Schmidt-Weber[3,4] | Joachim J. Bugert[5,6] | Roman Wölfel[5,6] | Vincent Grass[1] | Sandra Essbauer[5] | Daniel Schnepf[7,8] | Oliver T. Keppler[6,9] | Florian W. R. Vondran[6,10] | Andreas Pichlmair[1,6] | Carolin Mogler[11] | Gregor Ebert[1,6] | Ulrike Protzer[1,6]

[1]Institute of Virology, Technical University of Munich/Helmholtz Munich, Munich, Germany | [2]Infectious Diseases Therapeutic Research Center, Korea Research Institute of Chemical Technology (KRICT), Daejeon, South Korea | [3]Center of Allergy & Environment (ZAUM), Technical University of Munich/Helmholtz Munich, German Research Center for Environmental Health, Munich, Germany | [4]German Center for Lung Research (DZL), Munich Partner Site, Munich, Germany | [5]Department of Viruses and Intracellular Pathogens, Bundeswehr Institute of Microbiology, Munich, Germany | [6]German Centre for Infection Research (DZIF), Partner Sites Munich and Hannover-Braunschweig, Munich, Germany | [7]Institute of Virology, Medical Center University of Freiburg, Freiburg, Germany | [8]Immunoregulation Laboratory, The Francis Crick Institute, London, UK | [9]Max von Pettenkofer Institute & Gene Center, Faculty of Medicine, University of Munich, Munich, Germany | [10]ReMediES, Department of General, Visceral and Transplant Surgery, Hannover Medical School, Hannover, Germany | [11]Institute of Pathology, Technical University of Munich, Munich, Germany

Correspondence: Chunkyu Ko (ckko@krict.re.kr) | Ulrike Protzer (protzer@tum.de)

Received: 2 July 2024 | **Revised:** 25 November 2024 | **Accepted:** 18 December 2024

Funding: This study was supported by the German Research Foundation (DFG) via SFB-TRR179 (project 272983813 to U.P.), TRR22 (project 398577603 to C.S.W.) and TRR353 (project 471011418 to G.E.), by the State of Bavaria via research network FOR-COVID and Bay-VOC, by the project "Virological and immunological determinants of COVID-19 pathogenesis–lessons to get prepared for future pandemics" (KA1-Co-02 "COVIPA" to U.P.) and "Airborne Transmission of SARS Coronavirus - From Fundamental Science to Efficient Air Cleaning Systems" (KA1-Co-06 "CORAERO" to G.E.), grants from the Helmholtz Association's Initiative and Networking Fund, by the European Commission FET Open Grant VIROFIGHT (grant no. 899619), by the State of Bavaria and the European Union via a grant for regional infrastructure development (EFRE - REACT, to U.P. and G.E.), by the State of Bavaria via research networks FOR-COVID and Bay-VOC (to U.P. and O.T.K.) by the Federal Ministry of Education and Research (project ESCAPE; 01KI20169A to C.S.W.), and by the Medical Biological Defense Research Program of the Bundeswehr Medical Service (to J.J.B.). In addition, this research was supported by intramural funds from KRICT (project KK2432-10 and BSF24-111 to C.K.).

Keywords: ACE2 | COVID-19 | hepatocytes | liver | SARS-CoV-2 | TMPRSS2 | tropism

ABSTRACT

SARS-CoV-2 infection is accompanied by elevated liver enzymes, and patients with pre-existing liver conditions experience more severe disease. While it was known that SARS-CoV-2 infects human hepatocytes, our study determines the mechanism of infection, demonstrates viral replication and spread, and highlights direct hepatocyte damage. Viral replication was readily detectable upon infection of primary human hepatocytes and hepatoma cells with the ancestral SARS-CoV-2, Delta, and Omicron variants. Hepatocytes express the SARS-CoV-2 receptor ACE2 and the host cell protease TMPRSS2, and knocking down ACE2 and TMPRSS2 impaired SARS-CoV-2 infection. Progeny viruses released from infected hepatocytes showed the typical coronavirus morphology by electron microscopy and proved infectious when transferred to fresh cells, indicating that hepatocytes can contribute to virus spread. Importantly, SARS-CoV-2 infection rapidly induced hepatocyte death in a replication-dependent fashion, with the Omicron variant showing faster onset but less extensive cell death. C57BL/6 wild-type mice infected with a mouse-adapted SARS-CoV-2 strain showed high levels of viral RNA in liver and lung tissues. ALT peaked when viral RNA was cleared from the liver. Liver histology revealed profound tissue damage and immune cell infiltration,

Chunkyu Ko and Cho-Chin Cheng contributed equally to this work.

indicating that direct cytopathic effects of SARS-CoV-2 and immune-mediated killing of infected hepatocytes contribute to liver pathology.

1 | Introduction

Coronaviruses are enveloped viruses containing a positive-sense, single-stranded RNA genome of 26–32 kilobases (kb) and mostly cause self-limiting respiratory or gastrointestinal infections in humans and animals. The murine coronavirus, mouse hepatitis virus (MHV), is known to cause encephalitis and also hepatitis in susceptible rodents [1]. Coronaviruses have the capacity to adapt to a new host by genomic mutations and recombination that may lead to the emergence of new viruses that are infectious to humans or even highly virulent [2]. Recent examples include the severe acute respiratory syndrome coronavirus (SARS-CoV), the Middle East respiratory syndrome coronavirus (MERS-CoV), and, in late 2019, SARS-CoV-2. SARS-CoV-2 is highly transmissible and caused a worldwide pandemic with clinical pictures ranging from asymptomatic infection to severe respiratory illness and multiorgan damage termed coronavirus disease 2019 (COVID-19) [3].

SARS-CoV-2 enters the host cell after binding of the viral spike (S) protein to its host entry receptor angiotensin-converting enzyme 2 (ACE2) [4]. Upon binding to ACE2, the proteolytic cleavage of S by the host serine protease TMPRSS2 exposes the fusion peptide which mediates viral and cellular membrane fusion [5, 6] enabling intracellular viral replication. Early after infection, viral nonstructural proteins (NSPs) including the RNA-dependent RNA polymerase (RdRp; NSP12) are translated from the full-length genomic RNA (gRNA) and are responsible for the replication of the viral genome and the production of subgenomic RNAs (sgRNAs) that serve as templates to transcribe positive-sensed sg-mRNAs that are used for translation of structural and accessory proteins [7]. The structural proteins S, E (envelope), M (membrane), and N (nucleocapsid) are translated from sg-mRNAs.

The broad organotropism of SARS-CoV-2 is thought to contribute to severe COVID-19. SARS-CoV-2 RNA was detected in lung, kidney, liver, heart, brain, bowel and blood [8]. Acute kidney injury, vascular damage, cardiac dysfunction and neurological disorders, but also liver damage often become evident in patients with severe COVID-19 [9].

The liver is targeted by pathogens exploiting the fact that this vital organ provides an immunologically tolerant niche [10]. It is also involved in non-hepatotropic microorganisms spreading or causing systemic disease [11]. In COVID-19 patients, elevated aspartate (AST) and alanine aminotransferase (ALT) serum levels accompanied by modestly elevated total bilirubin levels are observed in 14.8%–53% of hospitalized patients [12], with a strong association between AST elevation, severe disease progression and mortality [13]. COVID-19 mortality is particularly high in patients with liver cirrhosis or pre-existing liver disease [14]. Direct SARS-CoV-2 infection of liver cells and secondary immunopathology may trigger ongoing liver disease as a long-term consequence of SARS-CoV-2 infection [15].

Analysis of human liver single-cell RNA sequencing (scRNA-seq) datasets revealed ACE2 expression in cholangiocytes (0.82%–14.29%) and hepatocytes (0.26%–10.2%) together with an increased expression of TMPRSS2 [16]. SARS-CoV-2 RNA was found in the lumen of the portal vein and surrounding endothelial cells by in situ hybridization [17], and coronavirus-like particles were detected by ultrastructural analysis of the liver tissue from COVID-19 patients [18]. Studies using liver organoids showed the permissiveness of hepatocytes and cholangiocytes to SARS-CoV-2 infection [19, 20], and SARS-CoV-2 was detected in and isolated from postmortem liver tissues [21, 22]. Recent studies demonstrated that SARS-CoV-2 is capable of infecting primary human hepatocytes (PHH) and hepatoma cells [22–25].

While these studies suggested a liver tropism of SARS-CoV-2, it has not been dissected how the virus enters hepatocytes and the extent and the consequence of virus replication within hepatocytes have remained open. We here show that the original EU strain B.1.177, as well as the Omicron variant B.1.1.529, productively infects PHH and induces cell death. Infected hepatocytes release infectious progeny virus and die as a consequence of the infection. In addition, we provide in vivo evidence for a liver tropism of SARS-CoV-2 using a physiological mouse model for COVID-19 that shows a pro-inflammatory cytokine response and develops liver damage presumably due to immune cell infiltration and subsequent viral clearance.

2 | Materials and Methods

2.1 | Cell Culture

PHH were obtained from the Department of General, Visceral, and Transplant Surgery at Hannover Medical School. PHH were freshly isolated and cultured as described elsewhere [26]. Alternatively, PHH were obtained from Thermo Fischer Scientific (Cat# HMCPIS). Liver tissue was processed from donors undergoing partial hepatectomy and upon obtaining written informed consent (approved by the ethics commission of Hannover Medical School, #252-2008). HepaRG, HepG2, and Huh7 cells were differentiated with DMSO before SARS-CoV-2 infection [27].

2.2 | SARS-CoV-2 Infection

A 2020 clinical isolate (European lineage B.1.177, EU1), the Delta variant (B.1.617.2), the Omicron variants (B.1.1.529, sub-lineage BA.1 and BA.5.1), and a mouse-adapted strain (MA20) [28] of SARS-CoV-2 were propagated in Vero-E6 cells. The identity of all viruses was verified via next-generation sequencing (GISAID database under accession ID: EPI_ISL_582134, EPI_ISL_2772700, EPI_ISL_7808190, and EPI_ISL_15942298). Cells were infected with SARS-CoV-2 strains at moi (multiplicity of infection) of 0.1–1

plaque-forming units (pfu)/cell for 1 h at 37°C, washed with PBS, and incubated with culture medium for the time indicated. During infection and maintenance of the cells, we did not observe any signs of dedifferentiation. siRNAs targeting siACE2 and siTMPRSS2 (*Silencer* Select siRNA; ID: s33966 and s14236) were delivered into cells using Lipofectamine RNAiMAX (both Thermo Fisher Scientific, Waltham, MA, USA).

8- to 10-week-old female C57BL/6J mice (Charles River Laboratories) were anesthetized with 2% isoflurane in O_2 and inoculated intranasally with 10^3 TCID50 of SARS-CoV-2 MA20 or 10^4 TCID50 of SARS-CoV-2 Omicron BA.5.1 in 40 μL PBS. Mice were monitored for clinical signs of disease and weighed daily. For sample acquisition and histological organ analysis, mice were euthanized. Experiments were conducted strictly according to the German regulations of the Society for Laboratory Animal Science and the European Health Law of the Federation of Laboratory Animal Science Associations. Experiments were approved by the District Government of Upper Bavaria (ROB-55.2-2532. Vet_02-21-169).

2.3 | Quantitative PCR (Rt-qPCR) of Viral and Cellular Rnas

RNA was extracted using the NucleoSpin RNA kit (Macherey-Nagel, Düren, Germany), and cDNA synthesis was performed with SuperScript III First-stand Synthesis System (Invitrogen; Thermo Fischer Scientific, Waltham, MA, USA). Quantitative PCRs were performed using LightCycler480 SYBR Green master-mix on a LightCycler480 Instrument (Roche, Mannheim, Germany). Primer sequences and qPCR conditions are described in Table S1.

2.4 | Protein Detection

Cells were harvested in RIPA buffer (Pierce; Thermo Fischer Scientific, Waltham, MA, USA) containing protease inhibitor cocktails. Proteins were separated by 10%–12% SDS-PAGE and blotted onto PVDF membrane. For enzymatic deglycosylation, 10 μL cell lysate was pretreated with 250 units of PNGase F (NEB, Frankfurt am Main, Germany) for 1 h. Membranes were incubated with following primary antibodies: anti-ACE2 (#ab108252 Abcam), anti-TMPRSS2 (sc-515727 Santa Cruz), anti-N (#40143-T62 Sino Biological), anti-GAPDH (#G9545 Sigma-Aldrich), anti-β-actin (#A5441 Sigma-Aldrich). Immunofluorescence staining was performed essentially as described [27] using SARS-CoV-2 anti-N antibody (#40143-T62 Sino Biological).

2.5 | Real-Time Live-Cell Imaging of SARS-CoV-2 Infected Hepatocytes

PHH were either mock or SARS-CoV-2 infected in the presence or absence of remdesivir (RDV) (1 μM), cultured in medium containing Incucyte Cytotox Red Reagent and monitored using the Incucyte Live-Cell Analysis System (Essen BioScience, Newark, UK). 25–36 phase contrast and fluorescence images/well/time point were taken every 4 h for 72 h, and analyzed using the Incucyte S3 software (version 2019B Rev2). Serial images taken from the same spots were combined to create time-lapse movies.

2.6 | Immunohistochemistry of Mouse Liver Tissues

Livers were fixed in 10% neutral-buffered formalin for 24 h, dehydrated and embedded in paraffin. 2 μm sections were stained with hematoxylin and eosin (H&E), or pretreated with EDTA buffer (pH 9.0) for 30 min, and stained with anti-SARS-CoV-2 S antibody (GeneTex, #135356, 1:1000, 15 min) and Bond Polymer Refine Detection Kit (Leica, Nussloch, Germany).

2.7 | Serum Analysis

Serum levels of interleukin (IL)-6 were measured using the Simple Plex Mouse Cytokine Panel (BioTechne, ST01C-MP-004435). ALT activity was determined on Reflovet Plus (Roche).

3 | Results

3.1 | Hepatocytes Express ACE2 and TMPRSS2

Given that ACE2 and TMPRSS2 play a key role in the cellular entry of SARS-CoV-2 [5], we analyzed ACE2 and TMPRSS2 mRNA expression in PHH isolated from four different donors, hepatoma cell lines HepG2, Huh7 and HepaRG, and lung-derived cell lines A549, BEAS-2B, 16HBE, and Calu-3. Primary normal human bronchial epithelial cells (NHBE), cell lines Caco-2 (human colorectal adenocarcinoma) and Vero-E6 (African green monkey kidney), known to be highly susceptible to SARS-CoV and SARS-CoV-2 infection [29], were included as controls (Figure 1A,B).

PHH showed high ACE2 mRNA levels comparable with those of Calu-3, Vero-E6 cells, and NHBE [30] (Figure 1A). Hepatoma HepG2 and Huh7 cells showed 10- to 14-fold lower ACE2 mRNA levels than PHH, and HepaRG cells showed the lowest ACE2 expression levels of the liver cells. Lung-derived cells had more divergent ACE2 mRNA levels with more than three orders of magnitude difference between Calu-3 and A549 cells (Figure 1A). TMPRSS2 mRNA expression levels in liver cells (except Huh7) exceeded those detected in lung-derived cells (Figure 1B), and absent in A549 and Vero-E6 cells, as reported earlier [31].

Western blot analysis confirmed ACE2 and TMPRSS2 expression on protein level. ACE2 was abundant in PHH, lower expressed in HepG2 and Huh7 cells and barely detectable in HepaRG cells (Figure 1C). TMPRSS2 was expressed in PHH, HepG2, and HepaRG cells and barely detectable in Huh7 cells. For TMPRSS2, besides the full-length protein at ~65 kDa, we detected a protein species of ~37 kDa, most likely representing the C-terminal trypsin-like S1 peptidase domain that has undergone activation by autocatalytic cleavage as described before [32, 33]. In PHH, ACE2 was modified by N-linked glycosylation, as evidenced by the selective removal of N-linked glycans by

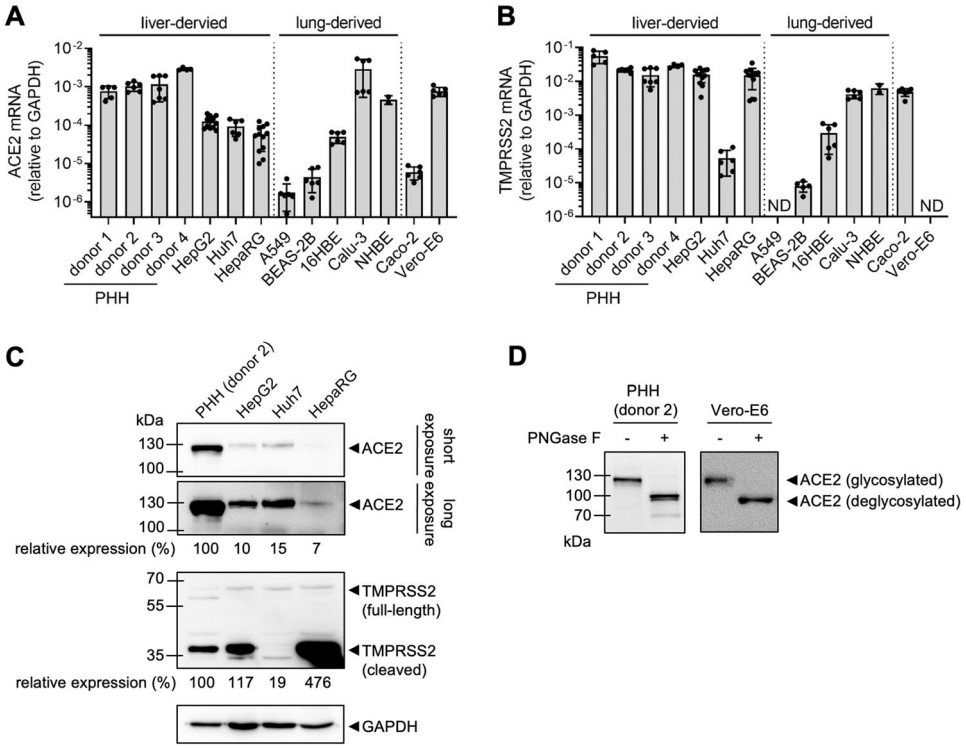

FIGURE 1 | ACE2 and TMPRSS2 expression profiles of different cell types. (A, B) The gene expression of ACE2 (A) and TMPRSS2 (B) of eleven different cell types was assessed by RT-qPCR. ACE2 and TMPRSS2 mRNA levels were normalized to GAPDH mRNA levels. Four different batches of PHH derived from individual donors were included in this analysis. (C) ACE2 and TMPRSS2 protein expression in liver-derived cell types was analyzed by Western blot analysis under reducing conditions. Protein band intensities were quantified using Multi Gauge software (V3.0) and normalized to GAPDH, which served as a loading control. The relative expression values are shown below the images. (D) Total cell lysate obtained from PHH and Vero-E6 cells were mock-treated or treated with PNGase F and subjected to Western blot analysis for the detection of ACE2. ND, not detected; RT-qPCR, reverse transcription quantitative PCR.

PNGase F (Figure 1D). The N-glycosylated form of ACE2 is known as the functional SARS-CoV receptor [34]. Taken together, we demonstrate expression of functional ACE2 and TMPRSS2 in human hepatocytes encouraging us to investigate whether hepatocytes support productive SARS-CoV-2 replication.

3.2 | Hepatocytes Support SARS-CoV-2 Replication

Probes or primers binding to the N-gene contained in the common regions of all SARS-CoV-2 RNAs allow the simultaneous detection of all viral RNA species. Northern blot analysis using an N-probe detected variable lengths of viral RNA species in PHH and Calu-3 cells following infection with the SARS-CoV-2 EU1 strain (EU1) (Figure 2A). As expected [35], N transcripts (~1.6 kb) were most abundant. RNA expression pattern in infected PHH was comparable to that in Calu-3 cells indicating intracellular SARS-CoV-2 replication in hepatocytes. However, due to sensitivity issues, we could not detect all viral RNA species, including the full-length gRNA (~30 kb).

Quantification of viral RNAs by RT-qPCR corroborated SARS-CoV-2 replication in liver cells, which was blocked by RDV, a potent nucleotide analog targeting the coronavirus RdRp and resulting in premature termination of viral RNA synthesis [36] (Figure 2B). PHH (although with some donor-to-donor variation), HepG2, and Huh7 cells supported robust SARS-CoV-2 replication. In contrast, HepaRG cells were considerably less permissive to SARS-CoV-2 (Figure 2B). The remaining viral RNAs after RDV treatment most likely resulted from either input gRNA or incomplete viral RNA sequences synthesized under RDV treatment.

Hepatic SARS-CoV-2 replication was also confirmed by detecting N protein, the most abundant protein produced upon infection with SARS-CoV-2 [37]. When PHH were infected with EU1, a strong N protein band was detected by Western blot analysis (Figure 2C). N protein-expressing cells became visible using immunofluorescence staining in PHH (Figure 2D) as well as in hepatoma cell lines (Figure 2E). Permissiveness of PHH to SARS-CoV-2 variants was reproduced by infecting PHH with the SARS-CoV-2 Omicron sublineage BA.1 (Omicron). Viral RNA, N protein, and N-positive cells were readily detectable (Figure 2F-G). In summary, our results demonstrated that SARS-CoV-2 efficiently replicates in hepatocytes, consistent with a recent finding showing the susceptibility of hepatoma cells to SARS-CoV-2 infection [25].

3.3 | SARS-CoV-2 Exploits ACE2 and TMPRSS2 to Infect Hepatocytes

To determine the essential role of ACE2 and TMPRSS2 for SARS-CoV-2 entry into hepatocytes, we transfected PHH with chemically modified siRNAs to knock down ACE2 or TMPRSS2

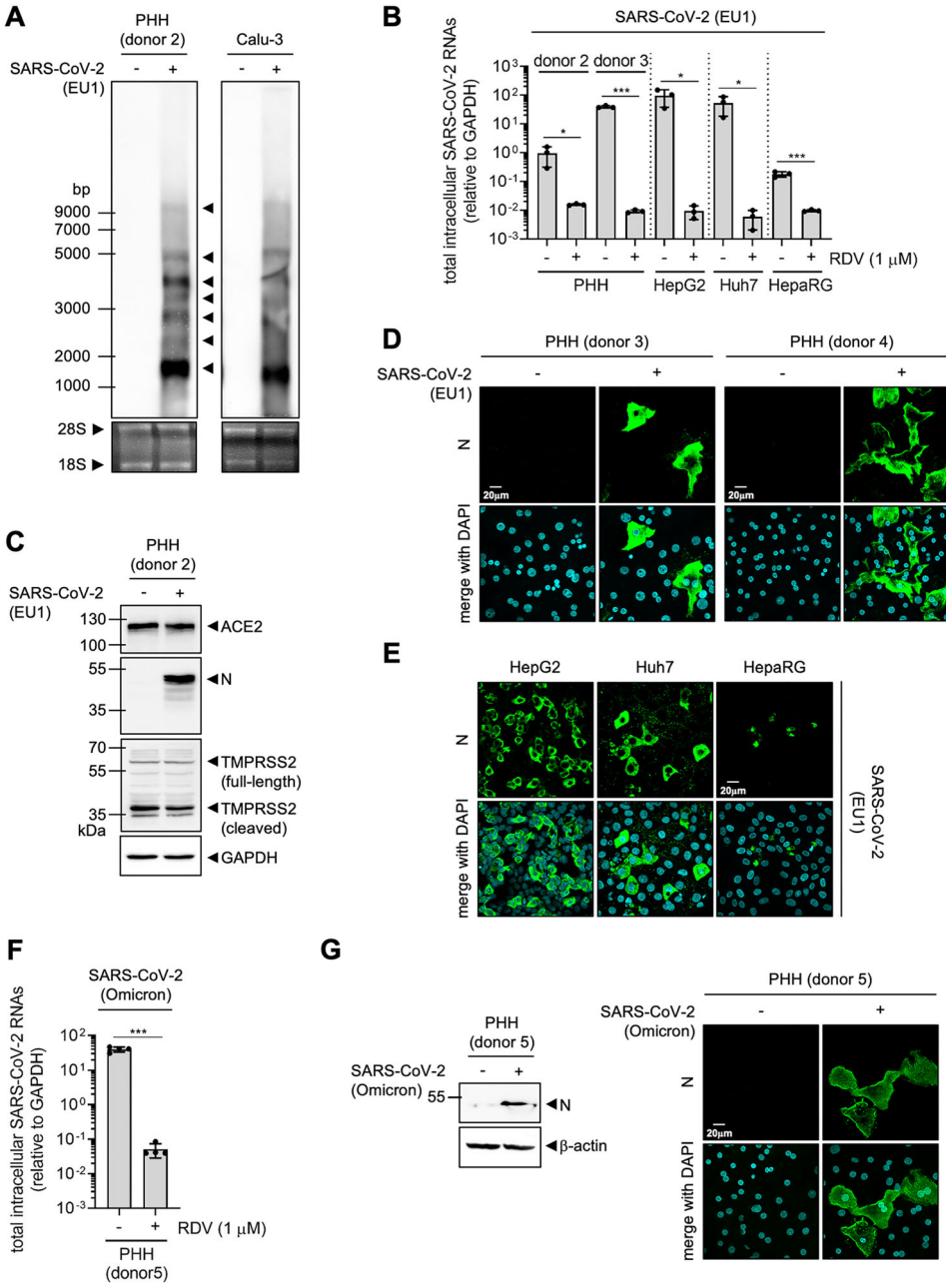

FIGURE 2 | Analysis of SARS-CoV-2 replication in hepatocytes. Cells were mock-infected or infected with SARS-CoV-2 (EU1 or Omicron) at an moi of 0.1 pfu/mL for PHH, HepG2, Huh7, Calu-3 cells. HepaRG cells were infected at an moi of 1 pfu/mL. Cells were collected at 24 h postinfection for the following analysis. (A) Intracellular SARS-CoV-2 RNA species were detected by Northern blot analysis with a digoxigenin-labeled double-stranded SARS-CoV-2 DNA probe complementary to N ORF. 28S and 18S ribosomal RNAs were used for loading control. Arrowhead heads indicate subgenomic (sg) RNAs. Single-stranded RNA ladders were used as a size-marking standard. (B) Intracellular SARS-CoV-2 RNA levels from untreated control and RDV-treated samples were analyzed by RT-qPCR using primers to N gene and were normalized to cellular GAPDH contents. (C) Antigen expression of SARS-CoV-2 was assessed in PHH. Western blot analysis detected ACE2, TMPRSS2, and SARS-CoV-2 N protein. GAPDH served as a loading control. (D, E) SARS-CoV-2 N protein expressing cells were visualized by indirect immunofluorescence staining. DAPI is used as a nuclear counterstain. Bars represent 20 μM. (F, G) Following SARS-CoV-2 (Omicron) infection to PHH, SARS-CoV-2 RNA and protein contents were analyzed as similar to panel (B–D). EU1, European lineage B.1.177; moi, multiplicity of infection; N, nucleocapsid; Omicron, Omicron variant (B.1.1.529); ORF, open reading frame; pfu, plaque-forming units; RDV, remdesivir; RT-qPCR, reverse transcription quantitative PCR. Statistical significance was determined using Student's *t*-test (***, $p \leq 0.001$; *, $p \leq 0.05$).

3 days before infection. Silencing of ACE2 and TMPRSS2, compared to control siRNA, reduced mRNA levels by 69% and 88%, respectively (Figure 3A). Reduction of total intracellular SARS-CoV-2 RNAs levels by 94% in siACE2-transfected cells and by 78% in siTMPRSS2-transfected cells showed that ACE2 and TMPRSS2 are essential for viral entry. Hereby, silencing of ACE2 had a dominant effect, although the knockdown efficiency of ACE2 was lower than that of TMPRSS2.

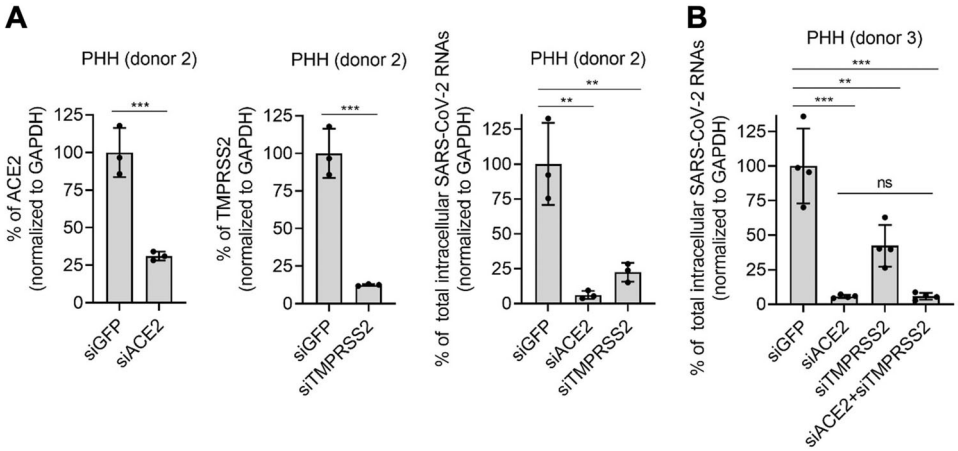

FIGURE 3 | The role of ACE2 and TMPRSS2 in SARS-CoV-2 infection of hepatocytes. (A) PHH were transfected with either siRNA against ACE2 (siACE2) or TMPRSS2 (siTMPRSS2) or control siRNA targeting GFP sequence (siGFP) at the final concentration of 300 nM. After 3 days, cells were additionally infected with SARS-CoV-2 (EU1) at an moi of 0.1 pfu/mL. After 24 h, the knockdown efficiency of ACE2 and TMPRSS2 mRNA was determined by RT-qPCR. The total intracellular SARS-CoV-2 RNA levels were measured by RT-qPCR with an N gene primer set. Cellular and viral RNA contents were normalized to GAPDH mRNA and set relative to siGFP used as control. (B) Another batch of PHH, similar to panel A, was used for SARS-CoV-2 infection following siRNA transfection. The sample cotransfected with siACE2 and siTMPRSS2 was included. EU1, European lineage B.1.177; moi, multiplicity of infection; N, nucleocapsid; pfu, plaque-forming units; RT-qPCR, reverse transcription quantitative PCR. Statistical significance was determined using Student's *t*-test (***, $p \leq 0.001$; **, $p \leq 0.01$; ns, not significant).

In a second experiment, using PHH from a different donor, we silenced ACE2 and TMPRSS2 simultaneously to determine whether dual knockdown of ACE2 and TMPRSS2 would result in further inhibition of SARS-CoV-2 infection. Individual silencing of ACE2 or TMPRSS2 inhibited intracellular viral RNA synthesis to a comparable extent as observed before (Figure 3A), but dual-silencing had no additional effect (Figure 3B). Overall, this demonstrated that SARS-CoV-2 infection of hepatocytes depends on ACE2 and TMPRSS2 expression.

3.4 | Hepatocytes Produce Infectious SARS-CoV-2 Progeny

Since hepatocytes supported SARS-CoV-2 entry and replication, we wondered whether infected hepatocytes would produce and secrete infectious SARS-CoV-2. To visualize the progeny virions secreted, virus particles in the cell culture media of infected cells (PHH, HepG2, Huh7, and Vero-E6 cells) were concentrated by ultracentrifugation through a sucrose cushion and analyzed by transmission electron microscopy. We readily detected virus particles of round shape with a size of 82–193 nm, coated with distinct spike protrusions, called peplomers (Figure 4A). We did not observe any morphological differences in progeny virions produced from liver-derived or Vero-E6 cells except for some pleiomorphism [3]. On the surface of most progeny virions, peplomers were evenly distributed indicating intact SARS-CoV-2 virions.

To address the question whether SARS-CoV-2 particles secreted from hepatocytes were infectious, we subjected the supernatant of infected cells to a standard plaque assay. Typical plaque formation represented cell lysis initiated by a single infectious virion (Figure 4B). Plaque quantification indicated that HepG2 and Vero-E6 cells released higher titer of infectious SARS-CoV-2 than PHH or Huh7 cells (Figure 4B, right panel) and proved that hepatocytes support the complete SARS-CoV-2 life cycle from viral entry to secretion of infectious progeny virus.

3.5 | SARS-CoV-2 Infection Causes Hepatocyte Death

Numerous viruses induce the death of their target cells. The coronavirus-induced CPE is cell type- and tissue-specific [38], prompting us to examine if SARS-CoV-2 infection induces a CPE in hepatocytes. We infected PHH with the ancestral SARS-CoV-2 EU1 strain and the Delta and Omicron variants. We monitored changes in cellular morphology over 3 days in the presence or absence of RDV or nirmatrelvir (NIR), the antivirally active compound of Paxlovid. To stain dead cells, a fluorescent cyanine nucleic acid dye was employed, which binds to the DNA of late apoptotic cells [39]. In uninfected cells, real-time imaging showed the typical morphology of PHH with a cuboidal shape and one or two round nuclei with prominent nucleoli (Figure 5A). Following infection with SARS-CoV-2, cell death was observed at 72 h (h) postinfection (p.i.) (Figure 5A; see also Supplementary Movies). We quantified cell death by measuring the total area containing fluorescent objects within each image (Figure 5B). Treating infected cells with RDV or NIR prevented hepatocyte cell death completely (Figure 5A–C), demonstrating that it depended on SARS-CoV-2 replication.

In cells infected with EU1, the number of dead cells rapidly increased between 28 and 36 h p.i., accompanied by a 50% decrease in cell confluence (Figure 5A,B). Interestingly, Delta and Omicron infection led to a replication-dependent, faster onset of cell death occurring at 16 h p.i., compared to 24 h p.i. for EU1. For all strains, the number of dead cells peaked around

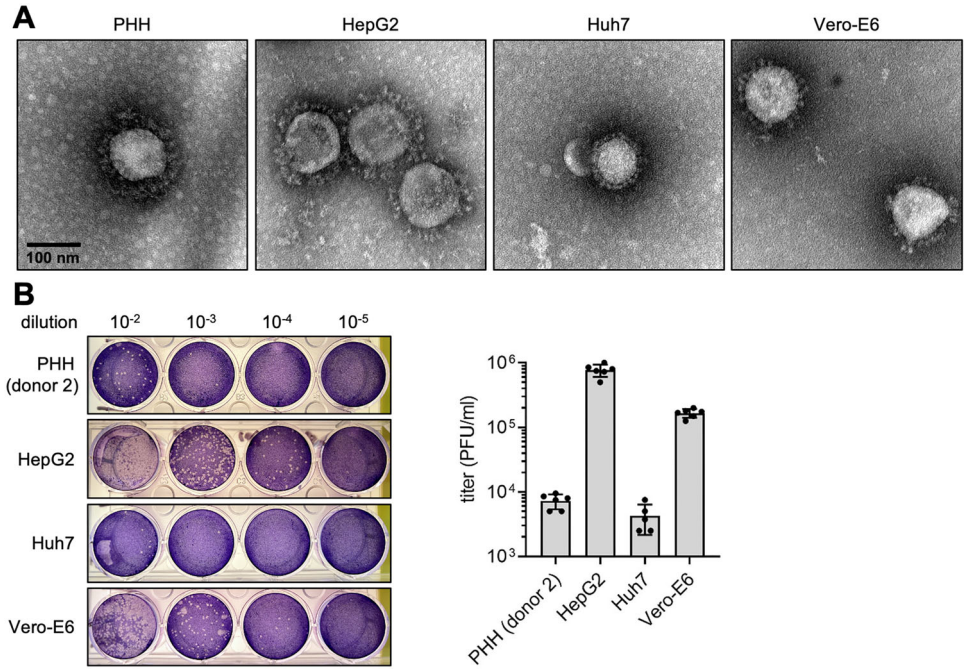

FIGURE 4 | Analysis of morphology and functionality of progeny virions produced from SARS-CoV-2 infected hepatocytes. Different cell lines (PHH, HepG2, Huh7 and Vero-E6) were infected with SARS-CoV-2 (EU1) at an moi of 0.1 pfu/mL. After 24 h, the supernatant was collected and clarified by low-seed centrifugation and either subjected to sucrose gradient ultracentrifugation to concentrate virus particles (A) or directly used to measure the infectious virus titer by plaque assay (B). (A) Transmission electron microscope images of negatively stained SARS-CoV-2 particles are shown. Scale 100 nm. (B) SARS-CoV-2 plaque phenotypes are shown in original color (left). The virus titer was determined as pfu/ml by counting the number of plaques at appropriate dilutions (right). EU1, European lineage B.1.177; moi, multiplicity of infection; pfu, plaque-forming units.

44 h p.i. and remained constant thereafter (Figure 5B). However, Delta and Omicron variants had a lesser effect on cell confluence, decreasing by 30% and 20%, respectively, highlighting differences in replication competence among SARS-CoV-2 strains. The gradual decrease of peak fluorescence signals likely reflects the degradation of stained DNA over time (Figure 5A). Overall, our results demonstrate that SARS-CoV-2 elicit a strong CPE in hepatocytes depending on viral replication.

3.6 | SARS-CoV-2 Infects the Liver of Mice

To validate hepatic tropism of SARS-CoV-2 in vivo, we infected C57BL/6J mice intranasally with the mouse-adapted MA20 strain [28]. We investigated the viral burden in the liver of animals at Days 3, 5, and 7 after infection by quantifying SARS-CoV-2 RNA copy numbers. We detected significant levels of SARS-CoV-2 in the liver of mice at Day 3, which was $2\log_{10}$ lower than in the lung. SARS-CoV-2 RNA copies decreased by Day 5 p.i., with only one of five animals still being SARS-CoV-2 RNA positive at Day 7 p.i. (Figure 6A). SARS-CoV-2 infection of the liver was confirmed by the staining of SARS-CoV-2 S protein (Figure 6B, left and Figure S1) with cholangiocytes remaining positive longer than hepatocytes (data not shown). A marked immune-cell infiltration of the infected liver was detected at day 5 p.i. (Figure 6B, right). A specific attraction of lymphocytes to sites of apoptotic events could not be detected, as staining of cleaved caspase 3 in liver tissue remained negative (data not shown). This indicated the clearance of SARS-CoV-2 infected hepatocytes by an adaptive immune response. High serum levels of IL-6 were detected that decreased alongside SARS-CoV-2 RNA over the course of the infection (Figure 6C). The reduction of SARS-CoV-2 RNA in the liver of mice until Day 7 p.i. also coincided with increasing serum ALT levels, indicating hepatocyte damage or death, potentially induced through the immune cell-mediated control of liver infection (Figure 6D). Other liver function markers were either undetectable in the serum or showed no significant increase with high variation between individual mice (Figure S2). Taken together, our results confirmed liver tropism of SARS-CoV-2 in mice accompanied by significant liver pathology.

4 | Discussion

Many SARS-CoV-2 infected patients have elevated liver enzymes, and patients with pre-existing liver diseases suffer from a more severe course of infection. We therefore systematically investigated SARS-CoV-2 infection of well-established, two-dimensional primary human hepatocytes and hepatoma cell cultures to define the entry mechanism of SARS-CoV-2 and its ability to replicate in and kill hepatocytes. In this study, we demonstrate that hepatocytes support the complete SARS-CoV-2 life cycle including the release of progeny virus that can infect new cells. Using live-cell time-lapse imaging, we detected a strong CPE in hepatocytes infected with SARS-CoV-2. In an in vivo model for SARS-CoV-2 infection, rapid liver infection with subsequent immune-cell infiltration and virus clearance

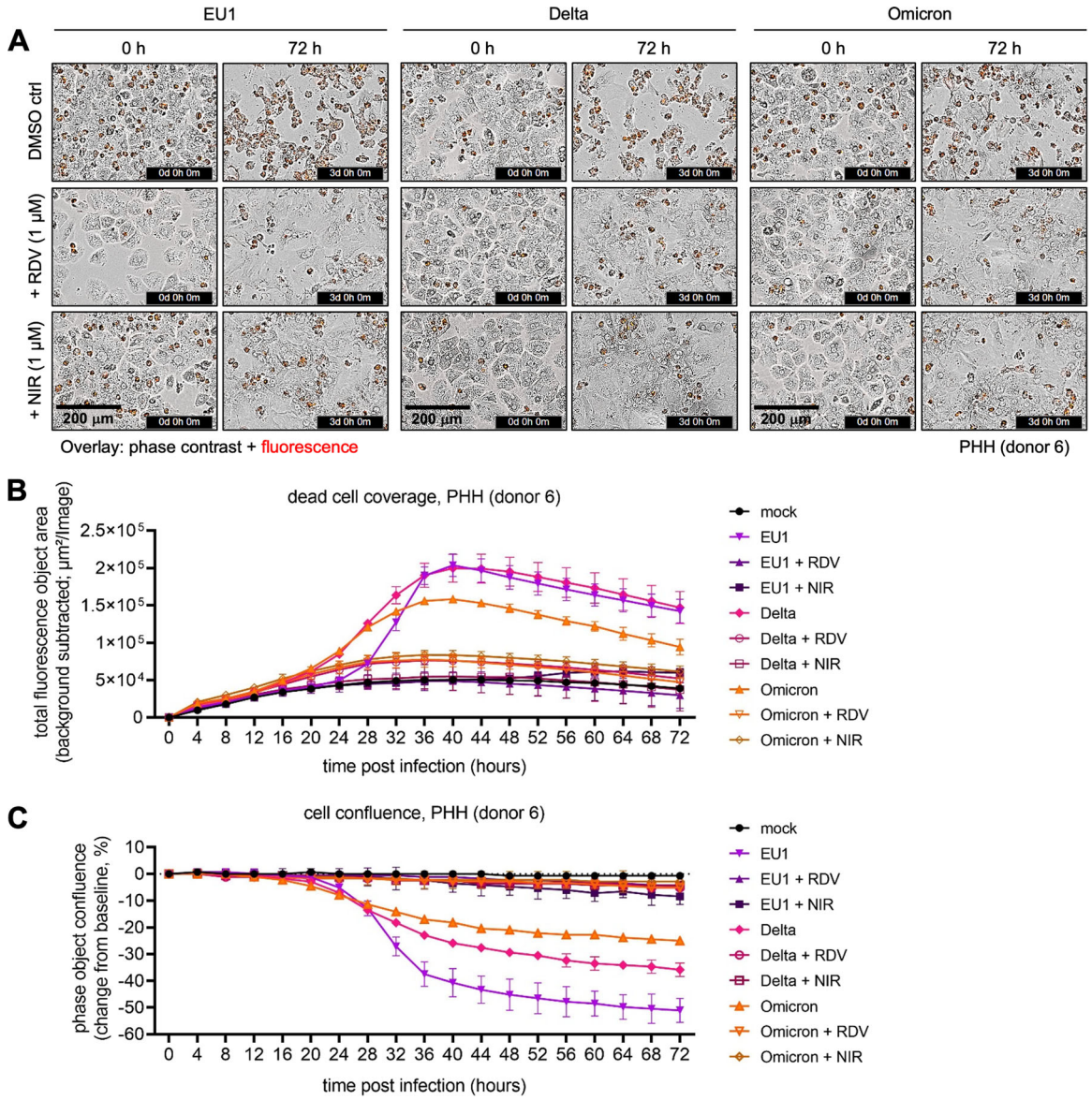

FIGURE 5 | Real-time imaging and quantitative analysis of hepatocytes infected with SARS-CoV-2. PHH were either left uninfected or infected with three different SARS-CoV-2 stains at a moi of 0.1 pfu/mL in the presence or absence of RDV (1 µM) or NIR (1 µM) for 1 h. After removing the inoculum (set as time zero), cells were cultured in the presence of Cytotox Red Dye for 72 h. RDV and NIR were continuously added after SARS-CoV-2 infection. Cells images were taken by automated, phase-contrast and fluorescence time-lapse microscope every 4 h for 72 h. (A) PHH were infected with SARS-CoV-2 EU1, Delta or Omicron. Overlays of fluorescence and phase contrast images of PHH taken at time 0 and 72 h are shown. (B) Background-subtracted total fluorescent objected area (μm^2/image) per experimental timeline is plotted as mean ± standard deviation. (C) Phase object confluence showing percentage (%) change from baseline is plotted as mean ± standard deviation. Scale bars represent 200 µm. Delta, Delta variant (B.1.617.2); EU1, European lineage B.1.177; moi, multiplicity of infection; NIR, nirmatrelvir; Omicron, Omicron variant (B.1.1.529); pfu, plaque-forming units; RDV, remdesivir. See also Supplementary Movies.

causing an ALT increase was observed. An accompanying serum ALT increase indicated immune-mediated virus clearance contributed to liver damage. As a result, the ALT increase in COVID-19 patients can be explained on the one hand by the death of infected cells through the CPE of SARS-CoV-2 and, on the other hand, by immune-mediated cell death during virus clearance.

Tissue tropism of viruses is primarily determined by receptor expression on the cell surface. ACE2 and TMPRSS2 are two critical host factors allowing SARS-CoV-2 entry into target cells [4, 5]. Recent studies analyzed the ACE2 expression profile in liver tissue by immunohistochemistry and reported that cholangiocytes show abundant ACE2 expression [40, 41], while hepatocytes seemed to express lower levels [40, 42]. Single-cell RNA sequencing [16, 41], demonstrated ACE2 expression in 1-14% of cholangiocytes and 0.3-10% of hepatocytes, respectively [16]. This led to a debate about whether hepatocytes might be permissive to SARS-CoV-2 infection and whether there might be technical limitations in detecting ACE2 in fixed tissue, resulting in an underestimation of ACE2 levels [21, 40, 43].

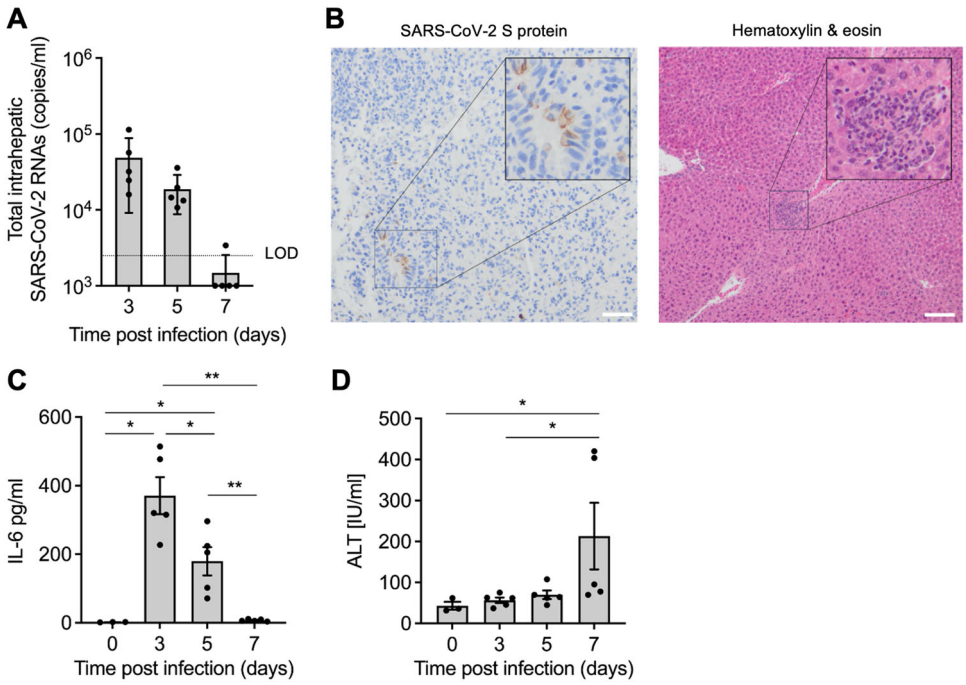

FIGURE 6 | Analysis of SARS-CoV-2 infection in mice. C57BL/6J mice were randomly allocated into one uninfected control group ($n = 3$) and three infected groups ($n = 5$, each). Mice were intranasally infected with 1×10^3 plaque-forming units of SARS-CoV-2 (MA20). Blood and livers were collected at 3, 5, and 7 days postinfection for the following analysis. (A) SARS-CoV-2 RNA was analyzed by qRT-PCR using primers targeting the nucleocapsid gene using a plasmid standard. (B) Mouse liver tissue collected at 5 days postinfection was stained with anti-SARS-CoV-2 spike antibody or hematoxylin and eosin. (C) IL-6 expression and (D) presence of ALT were assessed in the serum of mice. Mean and SEM are shown. Each dot represents an individual mouse. Data analysis was performed blinded to individual groups. Statistical significance was determined using Student's t test (**, $p \leq 0.01$; *, $p \leq 0.05$). The scale bar represents 50 μm. LOD: limit of detection.

Yang et al. hypothesized a hepatic SARS-CoV-2 infection through asialoglycoprotein receptor 1 (ASGR1)-dependent but ACE2-independent mechanisms [23]. Our data clearly demonstrate that ACE2 and TMPRSS are crucial entry factors. We could readily detect ACE2 and TMPRSS2 mRNA by RT-qPCR and protein by Western blot analysis in PHH isolated from different donors and all hepatoma cell lines analyzed. Interestingly, the gene expression levels were comparable to that in Calu-3 and Vero-E6 cells, two cell lines well-characterized to support robust SARS-CoV-2 infection. Targeted gene knockdown using siRNA lead us to define an ACE2- and TMPRSS2-dependent SARS-CoV-2 entry into hepatocytes. Interestingly, TMPRSS2 knockdown in HepG2 cells did not inhibit viral RNA synthesis, while ACE2 knockdown did (data not shown), indicating an alternative entry pathways into HepG2 cells (e.g. ACE2-cysteine protease cathepsin L routes [44]).

In a growing number of studies, SARS-CoV-2 RNA has been detected in blood samples from infected patients, referred to as RNAemia associated with disease severity [45]. Although there is so far no proof that infectious virus particles reach the liver via the bloodstream, RNAemia increases the risk of infection of various organs [9]. We examined whether hepatocytes fully support productive SARS-CoV-2 infection and provided different levels of evidence that SARS-CoV-2 can replicate in hepatocytes. First, we detected different lengths of SARS-CoV-2 RNA species by Northern blot analysis. As only full-length gRNA is delivered into cells upon SARS-CoV-2 infection, sgRNA is only detected when the virus replicates. Antiviral therapy with RDV blocked the accumulation of newly synthesized viral RNA. Finally, the cell culture media collected from SARS-CoV-2 infected hepatocytes contained infectious virions as demonstrated by passaging of the virus and plaque formation, suggesting that the liver, once infected, could contribute to virus dissemination.

Recently, Barreto et al. reported that SARS-CoV-2 can productively infect PHH and that the viral entry process is mediated by ACE2 and GPR78 [22]. Heinen et al. reported donor-specific susceptibilities to SARS-CoV-2 infection in PHH accompanied by the upregulation of genes associated with necroptotic and apoptotic signaling pathways and inflammatory responses [24]. We here demonstrate that SARS-CoV-2 infection of hepatocytes induces cell death by monitoring the morphology of infected PHH and fluorescent labeling of dead cells. Virus-induced CPE only occurred when the virus replicates, suggesting that either viral component(s) produced during viral replication or pattern recognition of replication intermediates triggered hepatocyte death. Notably, the proportion of cells that remained uninfected appeared healthy. This explains the hepatocyte heterogeneity with respect to SARS-CoV-2 infection and is consistent with a previous study showing that only a few hepatocytes express SARS-CoV-2 N protein following infection at a given time point [23].

We observed differences in the onset of cell death and the number of dead cells among SARS-CoV-2 strains. EU1 showed a later onset of detectable cell death occurring at 24 h p.i., but the number of dead cells rapidly increased, peaking at 40 h p.i.

alongside with a 50% decrease in cell confluence. In contrast, Delta or Omicron infection led to an earlier onset of cell death at 16 p.i., with reductions in confluence by 30% and 20%, respectively. Our finding is consistent with a previous study in the human bronchi showing that Omicron replicates faster than the previous strains (e.g., ancestral strain, Alpha, and Beta), possibly due to Omicron's preference for an endosomal entry route [46].

A growing body of evidence indicates that SARS-CoV-2 induces cell death via multiple pathways and involving several viral proteins [47]. Our preliminary studies using chemical inhibitors of different cell death pathways indicated the involvement of apoptosis and ferroptosis in virus-mediated CPE (data not shown). However, additional detailed investigations are required to determine which specific cell death modalities are activated by SARS-CoV-2 in infected hepatocytes, which viral component(s) are responsible, and to which extent cytokine responses following pattern recognition of SARS-CoV-2 infection contribute to the observed CPE. Our results align with the observation of apoptotic hepatocytes and typical coronavirus particles in situ in the liver of two patients with COVID-19 [18]. Accordingly, Zhao et al. reported that SARS-CoV-2 infection resulted in the upregulation of proapoptotic factors (e.g., CARD8, STK4) and disruption of barrier and bile acid transporting functions of cholangiocytes using human liver ductal organoids [19]. Thus, our findings complement previous reports demonstrating that SARS-CoV-2 infection of the liver and subsequent virus-induced CPE contribute to the rise of ALT and an impairment of liver function in COVID-19 patients. This shall not disregard that nonviral factors such as underlying liver disease, systemic inflammation, and drug-induced liver toxicity are contributing to the variable extend of liver damage observed in COVID-19 patients.

Using a mouse-adapted SARS-CoV-2 strain [28] in a physiological in vivo infection model applying infection in wildtype mice we demonstrated that SARS-CoV-2 can infect the liver. We detected SARS-CoV-2 RNA and SARS-CoV-2 S protein in the liver of infected animals. However, the number of infected cells was limited. Positive staining for SARS-CoV-2 S protein was detected in both hepatocytes and cholangiocytes. However, the relative virus protein amount in the liver was too low to be detected by immunoblotting (data not shown). A moderate elevation of serum ALT activity was accompanied by a marked infiltration of immune cells detected by histology in liver sections and a drop in SARS-CoV-2 RNA levels in the liver. The findings in our mice representing a physiological infection model are consistent with a study reporting severe liver pathology with infiltration of mononuclear inflammatory cells in STAT1-deficient mice infected with a mouse-adapted SARS-CoV variant [48]. In rhesus macaques inoculated with SARS-CoV-2, a higher viral load in the liver was accompanied by histological alterations [49]. In humans, COVID-19 has also been associated with autoimmune hepatitis [50].

The ALT increase in our mice was accompanied by increasing serum levels of the pro-inflammatory cytokine IL-6, a feature of COVID-19 that is also frequently observed in hospitalized patients [12]. IL-6, predominantly produced by macrophages and monocytes, has been proposed to account for the hyperinflammation and the cytokine storm in COVID-19 patients [51, 52], and blocking IL-6 improves the outcome of severely ill COVID-19 patients [53]. Interestingly, IL-6 is the lead cytokine produced by liver macrophages, while other macrophages predominantly produce tumor necrosis factor [54]. One may thus speculate that liver infection contributes to the increase in systemic IL-6 levels and, thus, to the hyperinflammation observed in COVID-19. To which extent the CPE by SARS-CoV-2 and immune-cell mediated killing of infected liver cells contribute to the liver damage observed remains to be determined.

Taken together, our findings show the liver tropism of SARS-CoV-2 and virus-induced liver damage in vivo and indicate that antiviral therapy may benefit COVID-19 patients with signs of liver injury.

Author Contributions

C.K., U.P. designed the study. C.K., C.C., G.E. and U.P. wrote the manuscript. C.K., C.C., D.M., S.A., J.S., B.L., R.B., O.P., M.G., C.A.J., J.J.B., R.W., V.G., S.E., C.M., G.E. performed experiments and analyzed the data. S.V. performed large data analysis. A.H., C.S.W., D.S., O.T.K., F.W.R.V., A.P., G.E. contributed essential material and instrumentation. All authors reviewed and agreed to the final version of the manuscript.

Acknowledgments

We thank Martin Feuerherd for providing access to the cDNA of NHBE and Marianne Rocha-Hasler for assisting with mouse serum analysis. This study was supported by the German Research Foundation (DFG) via SFB-TRR179 (project 272983813 to U.P.), TRR22 (project 398577603 to C.S.W.) and TRR353 (project 471011418 to G.E.), by the State of Bavaria via research network FOR-COVID and Bay-VOC, by the project "Virological and immunological determinants of COVID-19 pathogenesis – lessons to get prepared for future pandemics" (KA1-Co-02 "COVIPA" to U.P.) and "Airborne Transmission of SARS Coronavirus - From Fundamental Science to Efficient Air Cleaning Systems" (KA1-Co-06 "CORAERO" to G.E.), grants from the Helmholtz Association's Initiative and Networking Fund, by the European Commission FET Open Grant VIROFIGHT (grant no. 899619), by the State of Bavaria and the European Union via a grant for regional infrastructure development (EFRE - REACT, to U.P. and G.E.), by the State of Bavaria via research networks FOR-COVID and Bay-VOC (to U.P. and O.T.K.) by the Federal Ministry of Education and Research (project ESCAPE; 01KI20169A to C.S.W.), and by the Medical Biological Defense Research Program of the Bundeswehr Medical Service (to J.J.B.). In addition, this research was supported by intramural funds from KRICT (project KK2432-10 and BSF24-111 to C.K.). Open Access funding enabled and organized by Projekt DEAL.

Ethics Statement

The experimental procedures involving mice were conducted strictly according to the German regulations of the Society for Laboratory Animal Science (GV-SOLAS) and the European Health Law of the Federation of Laboratory Animal Science Associations (FELASA). Experiments were approved by the District Government of Upper Bavaria (ROB-55.2-2532. Vet_02-21-169).

Conflicts of Interest

UP received grants from SCG Cell Therapy, and VirBio and personal fees from Abbott, Abbvie, Arbutus, Gilead, GSK, Leukocare, J&J, Roche, MSD, Sanofi, Sobi and Vaccitech. UP is a cofounder and shareholder of SCG Cell Therapy. The other authors declare no conflicts of

interest. CAJ reports research funding from the German Center for Lung Research and an issued patent "Bradykinin B2 receptor antagonist for treatment of SARS-CoV2-infection" (EP3909646A1).

Data Availability Statement

The data that support the findings of this study are available from the corresponding author upon reasonable request.

References

1. S. R. Weiss and S. Navas-Martin, "Coronavirus Pathogenesis and the Emerging Pathogen Severe Acute Respiratory Syndrome Coronavirus," *Microbiology and Molecular Biology Reviews* 69, no. 4 (2005): 635–664.

2. A. M. Alluwaimi, I. H. Alshubaith, A. M. Al-Ali, and S. Abohelaika, "The Coronaviruses of Animals and Birds: Their Zoonosis, Vaccines, and Models for SARS-CoV and SARS-CoV2," *Frontiers in Veterinary Science* 7 (2020): 582287.

3. N. Zhu, D. Zhang, W. Wang, et al., "A Novel Coronavirus From Patients With Pneumonia in China, 2019," *New England Journal of Medicine* 382, no. 8 (2020): 727–733.

4. P. Zhou, X. L. Yang, X. G. Wang, et al., "A Pneumonia Outbreak Associated With a New Coronavirus of Probable Bat Origin," *Nature* 579, no. 7798 (2020): 270–273.

5. M. Hoffmann, H. Kleine-Weber, S. Schroeder, et al., "SARS-CoV-2 Cell Entry Depends on ACE2 and TMPRSS2 and Is Blocked by a Clinically Proven Protease Inhibitor," *Cell* 181, no. 2 (2020): 271–280.e8.

6. S. Steiner, A. Kratzel, G. T. Barut, et al., "SARS-CoV-2 Biology and Host Interactions," *Nature Reviews Microbiology* 22 (2024): 206–225.

7. L. Yan, Y. Zhang, J. Ge, et al., "Architecture of a SARS-CoV-2 Mini Replication and Transcription Complex," *Nature Communications* 11, no. 1 (2020): 5874.

8. V. G. Puelles, M. Lütgehetmann, M. T. Lindenmeyer, et al., "Multiorgan and Renal Tropism of SARS-CoV-2," *New England Journal of Medicine* 383, no. 6 (2020): 590–592.

9. T. Marjot, G. J. Webb, A. S. Barritt, et al., "COVID-19 and Liver Disease: Mechanistic and Clinical Perspectives," *Nature Reviews Gastroenterology & Hepatology* 18, no. 5 (2021): 348–364.

10. U. Protzer, M. K. Maini, and P. A. Knolle, "Living in the Liver: Hepatic Infections," *Nature Reviews Immunology* 12, no. 3 (2012): 201–213.

11. R. Talwani, B. L. Gilliam, and C. Howell, "Infectious Diseases and the Liver," *Clinics in Liver Disease* 15, no. 1 (2011): 111–130.

12. L. Xu, J. Liu, M. Lu, D. Yang, and X. Zheng, "Liver Injury During Highly Pathogenic Human Coronavirus Infections," *Liver International* 40, no. 5 (2020): 998–1004.

13. Z. Ding, G. Li, L. Chen, et al., "Association of Liver Abnormalities With In-Hospital Mortality in Patients With Covid-19," *Journal of Hepatology* 74, no. 6 (2021): 1295–1302.

14. T. Marjot, A. M. Moon, J. A. Cook, et al., "Outcomes Following SARS-CoV-2 Infection in Patients With Chronic Liver Disease: An International Registry Study," *Journal of Hepatology* 74, no. 3 (2021): 567–577.

15. T. Marjot, C. S. Eberhardt, T. Boettler, et al., "Impact of COVID-19 on the Liver and on the Care of Patients With Chronic Liver Disease, Hepatobiliary Cancer, and Liver Transplantation: An Updated EASL Position Paper," *Journal of Hepatology* 77, no. 4 (2022): 1161–1197.

16. V. De Smet, S. Verhulst, and L. A. van Grunsven, "Single Cell RNA Sequencing Analysis Did Not Predict Hepatocyte Infection by SARS-COV-2," *Journal of Hepatology* 73, no. 4 (2020): 993–995.

17. A. Sonzogni, G. Previtali, M. Seghezzi, et al., "Liver Histopathology in Severe COVID 19 Respiratory Failure is Suggestive of Vascular Alterations," *Liver International* 40, no. 9 (2020): 2110–2116.

18. Y. Wang, S. Liu, H. Liu, et al., "SARS-CoV-2 Infection of the Liver Directly Contributes to Hepatic Impairment in Patients With Covid-19," *Journal of Hepatology* 73, no. 4 (2020): 807–816.

19. B. Zhao, C. Ni, R. Gao, et al., "Recapitulation of SARS-CoV-2 Infection and Cholangiocyte Damage With Human Liver Ductal Organoids," *Protein & Cell* 11, no. 10 (2020): 771–775.

20. L. Yang, Y. Han, B. E. Nilsson-Payant, et al., "A Human Pluripotent Stem Cell-Based Platform to Study SARS-CoV-2 Tropism and Model Virus Infection in Human Cells and Organoids," *Cell Stem Cell* 27, no. 1 (2020): 125–136.e7.

21. N. Wanner, G. Andrieux, P. Badia-i-Mompel, et al., "Molecular Consequences of SARS-CoV-2 Liver Tropism," *Nature Metabolism* 4, no. 3 (2022): 310–319.

22. E. A. Barreto, A. S. Cruz, F. P. Veras, et al., "COVID-19-Related Hyperglycemia Is Associated With Infection of Hepatocytes and Stimulation of Gluconeogenesis," *Proceedings of the National Academy of Sciences* 120, no. 21 (2023): e2217119120.

23. X. Yang, X. Zheng, Y. Zhu, et al., "Asialoglycoprotein Receptor 1 Promotes SARS-CoV-2 Infection of Human Normal Hepatocytes," *Signal Transduction and Targeted Therapy* 9, no. 1 (2024): 42.

24. N. Heinen, R. Khanal, S. Westhoven, et al., "Productive Infection of Primary Human Hepatocytes With SARS-CoV-2 Induces Antiviral and Proinflammatory Responses," *Gut* 73, no. 10 (2024): e14.

25. O. A. Smirnova, O. N. Ivanova, I. T. Fedyakina, et al., "SARS-CoV-2 Establishes a Productive Infection in Hepatoma and Glioblastoma Multiforme Cell Lines," *Cancers* 15, no. 3 (2023): 632.

26. M. Kleine, M. Riemer, T. Krech, et al., "Explanted Diseased Livers - a Possible Source of Metabolic Competent Primary Human Hepatocytes," *PLoS One* 9, no. 7 (2014): e101386.

27. C. Ko, A. Chakraborty, W. M. Chou, et al., "Hepatitis B Virus Genome Recycling and De Novo Secondary Infection Events Maintain Stable Cccdna Levels," *Journal of Hepatology* 69, no. 6 (2018): 1231–1241.

28. J. Beer, S. Crotta, A. Breithaupt, et al., "Impaired Immune Response Drives Age-Dependent Severity of Covid-19," *Journal of Experimental Medicine* 219, no. 12 (2022): e20220621.

29. H. Chu, J. F.-W. Chan, T. T.-T. Yuen, et al., "Comparative Tropism, Replication Kinetics, and Cell Damage Profiling of SARS-CoV-2 and Sars-Cov With Implications for Clinical Manifestations, Transmissibility, and Laboratory Studies of COVID-19: an Observational Study," *Lancet Microbe* 1, no. 1 (2020): e14–e23.

30. C. A. Jakwerth, M. Feuerherd, F. M. Guerth, et al., "Early Reduction of SARS-CoV-2-replication in Bronchial Epithelium By Kinin B(2) Receptor Antagonism," *Journal of Molecular Medicine* 100, no. 4 (2022): 613–627.

31. S. Matsuyama, N. Nao, K. Shirato, et al., "Enhanced Isolation of SARS-CoV-2 By TMPRSS2-Expressing Cells," *Proceedings of the National Academy of Sciences* 117, no. 13 (2020): 7001–7003.

32. D. E. Afar, I. Vivanco, R. S. Hubert, et al., "Catalytic Cleavage of the Androgen-Regulated TMPRSS2 Protease Results in Its Secretion By Prostate and Prostate Cancer Epithelia," *Cancer Research* 61, no. 4 (2001): 1686–1692.

33. B. J. Fraser, S. Beldar, A. Seitova, et al., "Structure and Activity of Human TMPRSS2 Protease Implicated in SARS-CoV-2 Activation," *Nature Chemical Biology* 18, no. 9 (2022): 963–971.

34. W. Li, M. J. Moore, N. Vasilieva, et al., "Angiotensin-Converting Enzyme 2 Is a Functional Receptor for the Sars Coronavirus," *Nature* 426, no. 6965 (2003): 450–454.

35. D. Kim, J.-Y. Lee, J.-S. Yang, J. W. Kim, V. N. Kim, and H. Chang, "The Architecture of SARS-CoV-2 Transcriptome," *Cell* 181, no. 4 (2020): 914–921.e10.

36. C. J. Gordon, E. P. Tchesnokov, E. Woolner, et al., "Remdesivir Is a Direct-Acting Antiviral That Inhibits Rna-Dependent Rna Polymerase From Severe Acute Respiratory Syndrome Coronavirus 2 With High Potency," *Journal of Biological Chemistry* 295, no. 20 (2020): 6785–6797.

37. Y. Finkel, O. Mizrahi, A. Nachshon, et al., "The Coding Capacity of SARS-CoV-2," *Nature* 589, no. 7840 (2021): 125–130.

38. Y. J. Tan, S. G. Lim, and W. Hong, "Regulation of Cell Death During Infection By the Severe Acute Respiratory Syndrome Coronavirus and Other Coronaviruses," *Cellular Microbiology* 9, no. 11 (2007): 2552–2561.

39. E. Griffin, A. Levina, and P. A. Lay, "Vanadium(V) tris-3,5-di-tert-butylcatecholato Complex: Links Between Speciation and Anti-Proliferative Activity in Human Pancreatic Cancer Cells," *Journal of Inorganic Biochemistry* 201 (2019): 110815.

40. F. Hikmet, L. Méar, Å. Edvinsson, P. Micke, M. Uhlén, and C. Lindskog, "The Protein Expression Profile of ACE2 in Human Tissues," *Molecular Systems Biology* 16, no. 7 (2020): e9610.

41. X. Chai, L. Hu, Y. Zhang, et al., "Specific ACE2 Expression in Cholangiocytes May Cause Liver Damage After 2019-nCoV Infection," *bioRxiv* (2020): 931766.

42. I. Hamming, W. Timens, M. Bulthuis, A. Lely, G. Navis, and H. van Goor, "Tissue Distribution of ACE2 Protein, the Functional Receptor for SARS Coronavirus. A First Step in Understanding SARS Pathogenesis," *Journal of Pathology* 203, no. 2 (2004): 631–637.

43. X. Song, W. Hu, H. Yu, et al, "Little to No Expression of Angiotensin-Converting enzyme-2 on Most Human Peripheral Blood Immune Cells but Highly Expressed on Tissue Macrophages," *Cytometry A* 103, no. 2 (2023): 136–145, https://doi.org/10.1002/cyto.a.24285.

44. T. P. Peacock, D. H. Goldhill, J. Zhou, et al., "The Furin Cleavage Site in the SARS-CoV-2 Spike Protein Is Required for Transmission in Ferrets," *Nature Microbiology* 6, no. 7 (2021): 899–909.

45. C. A. Hogan, B. A. Stevens, M. K. Sahoo, et al., "High Frequency of SARS-CoV-2 Rnaemia and Association With Severe Disease," *Clinical Infectious Diseases* 72, no. 9 (2021): e291–e295, https://doi.org/10.1093/cid/ciaa1054.

46. K. P. Y. Hui, J. C. W. Ho, M. Cheung, et al., "SARS-CoV-2 Omicron Variant Replication in Human Bronchus and Lung Ex Vivo," *Nature* 603, no. 7902 (2022): 715–720.

47. C. Yuan, Z. Ma, J. Xie, et al., "The Role of Cell Death in SARS-CoV-2 Infection," *Signal Transduction and Targeted Therapy* 8, no. 1 (2023): 357.

48. T. Mahlakõiv, D. Ritz, M. Mordstein, et al., "Combined Action of Type I and Type III Interferon Restricts Initial Replication of Severe Acute Respiratory Syndrome Coronavirus in the Lung but Fails to Inhibit Systemic Virus Spread," *Journal of General Virology* 93, no. Pt 12 (2012): 2601–2605.

49. H. Zheng, H. Li, L. Guo, et al., "Virulence and Pathogenesis of SARS-CoV-2 Infection in Rhesus Macaques: A Nonhuman Primate Model of COVID-19 Progression," *PLoS Pathogens* 16, no. 11 (2020): e1008949.

50. R. Abe, N. Hasegawa, S. Suzuki, et al., "Simultaneous Occurrence of Autoimmune Hepatitis and Autoimmune Hemolytic Anemia After COVID-19 Infection: Case Report and Literature Review," *Clinical Journal of Gastroenterology* 17, no. 4 (2024): 677–682.

51. A. C. Gordon, P. R. Mouncey, F. Al-Beidh, et al., "Interleukin-6 Receptor Antagonists in Critically Ill Patients With Covid-19," *New England Journal of Medicine* 384, no. 16 (2021): 1491–1502.

52. T. Liu, J. Zhang, Y. Yang, et al., "The Role of interleukin-6 in Monitoring Severe Case of Coronavirus Disease 2019," *EMBO Molecular Medicine* 12, no. 7 (2020): e12421.

53. S. A. Jones and C. A. Hunter, "Is IL-6 a Key Cytokine Target for Therapy in COVID-19?," *Nature Reviews Immunology* 21, no. 6 (2021): 337–339.

54. L. Li, L. Cui, P. Lin, et al., "Kupffer-Cell-Derived IL-6 Is Repurposed for Hepatocyte Dedifferentiation via Activating Progenitor Genes From Injury-Specific Enhancers," *Cell Stem Cell* 30, no. 3 (2023): 283–299.e9.

Supporting Information

Additional supporting information can be found online in the Supporting Information section.